OPEN ACCESS

Renewable Energy ARTICLE

The Innovation Energy

Construction and performance analysis of a hydrogen liquefaction precooling process integrating an active magnetic regenerator

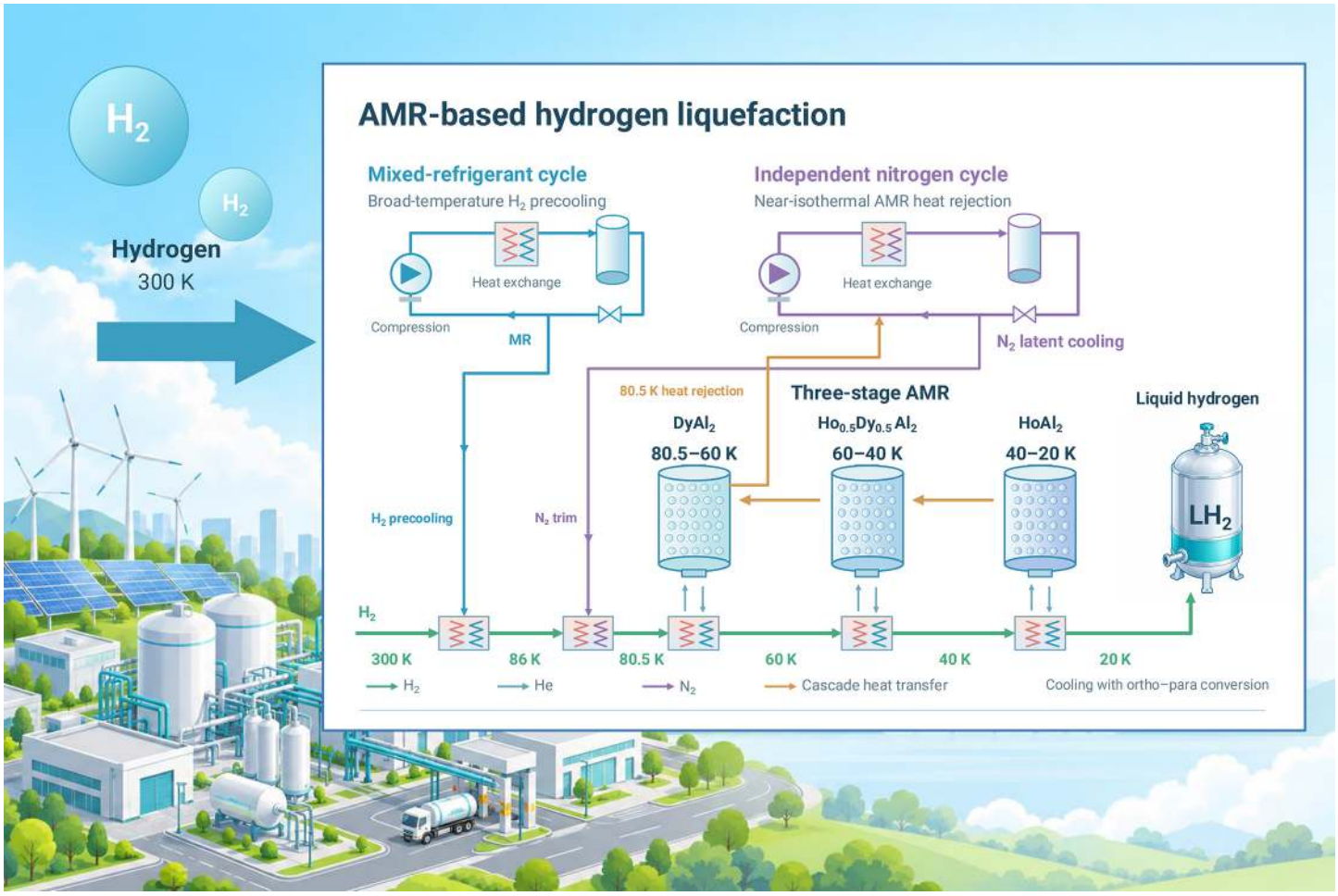
Zhouhang Hu,[1] Zhenxing Li,[1,4,*] Yakun Liu,[1] Jun Liu,[1,4] Huifang Kang,[1] Hang Li,[3] Hongwei Zhang,[4] Jiahui Wang,[1] and Jun Shen[1,2,4,*]

*Correspondence: zxli@bit.edu.cn (Z. L.); jshen@bit.edu.cn (J. S.)

Received: May 23, 2026; Accepted: September 9, 2026; Published Online: October 19, 2026; https://doi.org/10.59717/j.xinn-energy.2026.100187

© 2026 The Author(s). This is an open access article under the CC BY license (https://creativecommons.org/licenses/by/4.0/).

GRAPHICAL ABSTRACT



PUBLIC SUMMARY

- Conventional liquid-hydrogen transportation is hindered by low-efficiency, high-cost hydrogen liquefaction, and compressor-driven refrigeration faces stricter environmental-friendly requirements.
- This work proposes a hydrogen liquefaction scheme integrated with active magnetic regenerator (AMR), aiming for compact and high-efficiency small-scale liquefaction systems.
- Three precooling and hot-end heat-rejection layouts are built for a three-stage cascaded AMR system under identical hydrogen-supply and operating boundary conditions.
- Case Ⅲ delivers optimal overall performance with SEC of 62 kJ/g and COP of 0.072, benefiting from separating wide-range hydrogen precooling and AMR hot-end heat-rejection loads.
- The mixed-refrigerant cycle supplies wide-range sensible cooling for hydrogen, while an independent nitrogen circuit dissipates AMR hot-end heat, offering design guidance for AMR-based hydrogen liquefaction.

ARTICLE Renewable Energy

OPEN ACCESS

www.the-innovation.org/the-innovation-energy

Construction and performance analysis of a hydrogen liquefaction precooling process integrating an active magnetic regenerator

Zhouhang Hu,[1] Zhenxing Li,[1,4,*] Yakun Liu,[1] Jun Liu,[1,4] Huifang Kang,[1] Hang Li,[3] Hongwei Zhang,[4] Jiahui Wang,[1] and Jun Shen[1,2,4,*]

[1]School of Mechanical Engineering, Beijing Institute of Technology, Beijing 100081, China
[2]Technical Institute of Physics and Chemistry, Chinese Academy of Sciences, Beijing 100190, China
[3]Institute of Engineering Thermophysics, Chinese Academy of Sciences, Beijing 10090, China
[4]Energy and Transportation Domain, Beijing Institute of Technology (Zhuhai), Zhuhai 519088, China
*Correspondence: zxli@bit.edu.cn (Z. L.); jshen@bit.edu.cn (J. S.)

Received: May 23, 2026; Accepted: September 9, 2026; Published Online: October 19, 2026; https://doi.org/10.59717/j.xinn-energy.2026.100187

© 2026 The Author(s). This is an open access article under the CC BY license (https://creativecommons.org/licenses/by/4.0/).

Citation: Hu Z., Li Z., Liu Y., et al. (2026). Construction and performance analysis of a hydrogen liquefaction precooling process integrating an active magnetic regenerator. *The Innovation Energy* **3**:100187.

The transportation of liquid hydrogen faces significant challenges, primarily due to the low efficiency and high cost of conventional hydrogen liquefaction (HL) processes. Meanwhile, increasingly stringent environmental regulations impose higher demands on the energy efficiency and eco-friendliness of traditional compressor-based refrigeration technologies. In this context, magnetic refrigeration technology based on the active magnetic regenerator (AMR) has emerged as a promising alternative. Targeting the development of compact and high-efficiency HL systems, this paper proposes a HL process integrated with an AMR. The study focuses on the integration method of the AMR and the design and analysis of different cooling schemes. To evaluate the applicability of an AMR in small-scale HL, three precooling and hot-end heat-rejection configurations are constructed for the same three-stage cascaded AMR system. The three configurations share identical hydrogen feed conditions, liquefaction capacity, and AMR operating parameters, while differing only in the method used to precool hydrogen and reject heat from the high-temperature AMR hot end. The results show that Case III exhibits the best overall performance, achieving the lowest *SEC* (62 kJ/g) and the highest *COP* (0.072). The improved performance of Case III results from the functional separation of the broad-temperature hydrogen precooling load and the quasi-isothermal heat-rejection load of the high-temperature AMR. The MR cycle mainly provides sensible cooling for hydrogen over a wide temperature range, whereas the independent nitrogen cycle removes the AMR hot-end heat load near 80.5 K. These results provide guidance for the thermal integration and precooling design of small-scale AMR-based HL systems.

INTRODUCTION

Against the backdrop of a global energy transition toward low-carbon systems, hydrogen, with its zero-carbon emissions, high heating value, and renewability, is regarded as a key energy carrier for replacing fossil fuels and achieving carbon neutrality.[1–3] The International Energy Agency, in its Net Zero by 2050 roadmap, points out that hydrogen and hydrogen-based fuels will play an irreplaceable role in sectors where direct electrification is difficult or where sustainable bioenergy supply is limited.[4] However, the extremely low volumetric energy density of hydrogen poses significant challenges to its large-scale storage and long-distance transportation.[5–7] Liquid hydrogen, owing to its high volumetric energy density and fast refueling capability, is considered an important technological pathway to overcome the bottlenecks of hydrogen storage and transportation.[2] At present, commercial hydrogen liquefaction (HL) plants are mainly based on cryogenic refrigeration systems (e.g., Claude cycles) that rely on the Joule-Thomson effect or helium Brayton cycles.[8] Although these systems are technologically mature, they generally suffer from complex process configurations, high capital costs, and relatively low energy efficiency, leaving substantial room for improvement. Specifically, the exergy efficiency of existing liquefaction plants is merely 19.3%–23.1%, and compressor energy consumption accounts for over 80% of the total, indicating considerable optimization potential.[9–13]

The structure of hydrogen supply and demand systems is also undergoing changes. The market demand for hydrogen is rapidly evolving from the traditional centralized, large-scale model toward a diversified and distributed pattern—namely, a transition from centralized production and long-distance transportation to distributed hydrogen supply deeply coupled with renewable energy sources.[14] This transformation is driven by both supply and demand sides. On the supply side, wind and solar resources are geographically dispersed and are often concentrated in deserts, coastal areas, and other remote regions far from major demand centers. This spatial mismatch, together with limited grid integration capacity, frequently results in wind and solar power curtailment.[15-16] Converting surplus electricity into hydrogen via power-to-hydrogen routes has become an important means of improving renewable energy utilization. Water electrolysis can convert fluctuating electricity into transportable hydrogen, enabling cross-time-scale energy transfer and thus supporting long-duration energy storage and multi-energy coupling systems.[17] On the demand side, hydrogen applications are expanding from centralized scenarios to a variety of end-uses, exhibiting small-to-medium scale and spatial dispersion.[16] For example, in heavy-duty transportation, hydrogen demand is distributed across multiple discrete terminals such as ports, logistics parks, and trunk line transport nodes, forming a typical "multi-node, small-scale" pattern.[18] In off-grid or weak-grid scenarios such as islands, remote areas, and microgrids, hydrogen serves as an energy storage and regulation medium to enable low-carbon and autonomous operation of energy systems.[19] The synergistic evolution of these supply and demand structures imposes higher requirements on the flexibility and distributed capability of hydrogen supply systems, further driving the need for modular, small-scale, and high-efficiency HL equipment.

In this context, the development of small-scale HL technologies faces new opportunities and challenges. Although conventional gas-expansion cryogenic refrigeration cycles have been continuously optimized, the potential for further energy efficiency improvement is gradually diminishing. In contrast, magnetic refrigeration technology based on the magnetocaloric effect offers new possibilities for overcoming existing energy efficiency bottlenecks owing to its unique thermodynamic mechanism.[20] This technology relies on the magnetic entropy change of solid refrigerants, and its theoretical efficiency approaches the Carnot limit,[21] providing potential advantages in reducing the specific energy consumption (*SEC*) of small-scale liquefaction equipment. Experimental and numerical studies have demonstrated that active magnetic regenerator (AMR) systems can achieve relatively high fractions of Carnot performance in the cryogenic temperature range, indicating their potential for compact and small-scale HL applications.[22-23] Furthermore, magnetic refrigeration systems do not rely on high-pressure gas expansion or high-speed rotating machinery, making them relatively simple in structure and helping to reduce vibration and maintenance requirements, which is advantageous for distributed and unattended scenarios. However, most existing studies use magnetic refrigeration only as a precooling stage for conventional cycles, without fully exploiting its potential in deep-cryogenic liquefaction processes.[9,24-25] In particular, direct liquefaction pathways based on magnetic refrigeration in the liquid hydrogen temperature range (around 20 K) are still in the exploratory stage, and the system configurations and performance limits require further investigation.[26]

At the system implementation level, equating an AMR operating in the liquid hydrogen temperature range to a cryogenic refrigerator in a specific temperature range is a common approach for thermodynamic analysis. However, the heat rejection from its hot end constitutes a critical engineering issue. While providing cryogenic cooling, the hot end of the AMR (around 80

K) must continuously reject heat;[27] therefore, an efficiently matched heat rejection scheme has a decisive impact on system performance. Currently, liquid nitrogen precooling or external cryocoolers (e.g., GM cryocoolers) are often used for hot-end cooling.[22,28] However, the liquid nitrogen scheme relies on consumable working fluids, increasing operating costs and introducing upstream exergy losses;[29] external cryocoolers suffer from poor temperature matching, leading to significant irreversible exergy losses during heat exchange. Therefore, developing an integrated precooling system that matches the heat load characteristics of the AMR hot end and enables efficient cooling over a wide temperature range is of great importance for improving overall energy efficiency and promoting the engineering application of magnetic refrigeration HL technology.

This study focuses on the thermal integration of a fixed three-stage AMR system for small-scale HL, rather than a general comparison with conventional liquefaction technologies. The three cases differ only in the precooling and AMR hot-end heat-rejection strategy. Based on different precooling strategies, three typical precooling architectures are constructed, compared, and analyzed: (I) an open-cycle precooling process using liquid nitrogen; (II) a closed-cycle precooling process based on a single MR cycle; (III) a dual-cycle precooling process coupling a mixed refrigerant (MR) cycle with an independent nitrogen cycle. Methodologically, the steady-state operating characteristics of a three-stage cascaded AMR in the target temperature range of 20–80.5 K are first determined via numerical simulation. On this basis, complete steady-state process models coupling each precooling scheme with the AMR system are established using Aspen Plus, and systematic energy and exergy analyses are conducted. This paper further focuses, from a thermodynamic perspective, on the intrinsic mechanisms by which the dual-cycle precooling process reduces system power consumption and improves the utilization efficiency of energy quality. The results can provide a theoretical basis and technical pathway for the design of efficient and small-scale magnetic refrigeration HL systems.

MATERIALS AND METHODS

AMR refrigeration performance simulation

Description of AMR simulation. In this study, a three-stage cascaded AMR system is adopted. The operating temperature ranges of the three stages are set as 20-40 K (low-temperature stage), 40-60 K (medium-temperature stage), and 60-80.5 K (high-temperature stage).[27] To ensure a sufficient heat exchange temperature difference between the hot end of the high-temperature stage AMR and the precooling working fluid, the hot-end temperature of the high-temperature stage AMR is set to 80.5 K, which is 0.5 K higher than the 80 K adopted by Zheng et al. This system employs a cascaded thermal coupling design: the cold end of the high-temperature stage AMR cools the hot end of the medium-temperature stage, and the cold end of the medium-temperature stage further cools the hot end of the low-temperature stage. Meanwhile, each stage independently provides the required cooling load for HL. Thus, the system achieves refrigeration across a wide temperature range from 20 K to 80.5 K.

The AMR refrigeration performance simulation initiates from the hot end. A precooling system establishes a hot-end temperature of approximately 80.5 K for the high-temperature stage AMR. Based on this, the three-stage AMR operates sequentially to realize cascade cooling, ultimately aiming to achieve a low-temperature level at the cold end of the low-temperature stage that is appropriate for liquid hydrogen production. To quantitatively evaluate the cooling performance of this cascaded system, independent numerical simulations are conducted for each AMR stage. The relevant physical models are based on reasonable simplifying assumptions, and the governing equations along with boundary conditions are clearly defined. Helium is selected as the heat transfer fluid, and the magnetizing source is a Halbach-type permanent magnet array with a maximum magnetic field intensity of 1 T. The simulation adopts the active magnetic Brayton cycle.

In this AMR model, $HoAl_2$ is used for the low-temperature stage, $Ho_{0.5}Dy_{0.5}Al_2$ for the medium-temperature stage, and $DyAl_2$ for the high-temperature stage.[30-31] The density, specific heat capacity, thermal conductivity, and dynamic viscosity of helium are all functions of temperature and pressure, which are calculated using the REFPROP database. Nielsen et al. reported that particle diameter is strongly coupled with cycle frequency and fluid utilization, with smaller dimensions enhancing heat transfer at the expense of increased pressure drop.[32] The particle diameter is selected to ensure sufficient solid–fluid heat transfer within the 1 s cycle.

Boundary conditions and output parameters. In the simulation, the initial hot-end temperature of the AMR is set to 80.5 K, and the cold-end temperature is set to 60 K. The temperatures at other positions are uniformly distributed along the axial direction. When the helium mass flow rate is negative, helium is pumped from the cold end through the regenerator to the hot end (hot-blow process). In this case, the inlet boundary condition at the cold end is $T_f = T_c$, and the outlet boundary condition at the hot end is $\partial T_f / \partial z = 0$. Conversely, when the helium mass flow rate is positive, helium is pumped from the hot end through the regenerator to the cold end (cold-blow process). Then, the inlet boundary condition at the hot end is $T_f = T_h$, and the outlet boundary condition at the cold end is $\partial T_f / \partial z = 0$. Here, the z-axis is the axial direction of the regenerator.

Based on the above governing equations, a transient study is performed in COMSOL Multiphysics 5.5 using the PARADISO direct solver. After reaching the steady state, the following performance parameters can be calculated from the model output data: cooling capacity Q_c, heat rejection Q_h, and pumping work W_p (the work consumed for pumping helium). The calculation methods are as follows:

$$Q_c = \frac{\int_0^\tau |m_f(t)|\, c_{p,f}\,[T_c - T_{f,cold}(t)]\, dt}{\tau} \tag{1}$$

$$Q_h = \frac{\int_0^\tau |m_f(t)|\, c_{p,f}\,[T_{f,hot}(t) - T_h]\, dt}{\tau} \tag{2}$$

$$W_p = \frac{1}{\tau}\int_0^\tau \frac{|m_f(t)\Delta p(t)|}{\rho_f} dt \tag{3}$$

where $T_{f,cold}(t)$ is the helium outlet temperature at the cold end, $T_{f,hot}(t)$ is the helium outlet temperature at the hot end, and $\Delta p(t)$ is the pressure drop when helium flows through the regenerator.

Simulation results. This study targets small-scale HL refrigeration equipment. Therefore, the subsequent operating condition design and optimization are based on a liquefaction capacity of 1.2 kg/d. For this liquefaction capacity, the cooling capacity required at the cold head is approximately 10 W. Following the above procedure, the three-stage AMR is simulated, and the cooling capacity matching is performed. In addition to providing the cooling capacity required at the hot end of the next-stage AMR, the high-temperature and medium-temperature stages must also supply the heat required for hydrogen cooling and ortho-to-para hydrogen conversion. Since the same magnet assembly is used for all three stages, the same blow coefficient is adopted for the matched operating conditions. In this study, the utilization factor U is taken as 0.8 for all stages, and its definition is given in Equation (4):

$$U = \frac{\int_0^\tau |m_f(t)|\, c_{p,f} dt}{2 m_s c_{p,s}} \tag{4}$$

The cooling capacity, heat rejection, pumping work, and operating parameters of each matched AMR stage are summarized in Table 1.

The high pumping work of the high-temperature-stage AMR is mainly attributed to the relatively small magnetic entropy change of $DyAl_2$, which requires more magnetocaloric material per unit cooling capacity. Consequently, this stage employs a larger regenerator and higher helium circulation, and the total pressure drop of the cascaded AMR is dominated by Δp across the high-temperature regenerator, resulting in a pumping work of 236.6 W. Increasing the particle diameter d or reducing the utilization factor U may lower the flow resistance and pumping work, but may also weaken heat transfer and cooling performance, while the effect of L/D depends on the coupled changes in flow length and cross-sectional area. Therefore, these parameters require coordinated optimization. However, detailed optimization of the regenerator geometry is beyond the scope of this study, which focuses on precooling integration.

Hydrogen liquefaction process description

Simulation parameters. Among the available technical routes for ortho-to-

Table 1. Summary of simulation results for each AMR stage

Parameter	Low-temperature stage AMR	Medium-temperature stage AMR	High-temperature stage AMR
Cooling capacity (W)	10.7	33.23	61.37
Heat rejection (W)	26.41	55.94	83.97
Pumping work (W)	0.94	49.96	236.6
Operating conditions	t=1s, v=4×10^{-5}m^3, m=156.67g, L/D=3.5, U=0.8, d=0.1mm, $HoAl_2$	t=1s, v=4×10^{-5}m^3, m=155.39g, L/D =3.5, U=0.8, d=0.05mm, $Ho_{0.5}Dy_{0.5}Al_2$	t=1s, v=6×10^{-5}m^3, m=230.4g, L/D =3.5, U=0.8, d=0.1mm, $DyAl_2$

para hydrogen conversion, the continuous conversion method has clear advantages due to its simple structure and low requirement for manual intervention; thus, this method is adopted in the present study. This method integrates the conversion process directly inside the heat exchanger without requiring a separate reactor. The catalyst is placed on one side of the heat exchanger, i.e., in the flow channel where hydrogen is cooled, thereby achieving simultaneous cooling and conversion. According to the design of this study, the catalyst is installed at the hot end of the heat exchanger. In this study, the feed hydrogen pressure is set to 101.325 kPa, and the temperature is set to 300 K, with an ortho-hydrogen concentration of 74.93% and a para-hydrogen concentration of 25.07%. The physical properties of ortho-hydrogen, para-hydrogen, and other working fluids are obtained from the Aspen Properties database. Because of the wide range of temperatures and pressures, the availability of a complete binary interaction parameter database, and the ease and speed of calculation, the Peng-Robinson equation of state is used for this process. In this paper, the hot end of the heat exchanger is set to simulate the process and reaction, as shown in Equation (5):[33-34]

$$o\text{-}H_2 \rightarrow p\text{-}H_2 + \Delta H_c \quad (5)$$

Aspen Plus V14 is used to perform steady-state simulations of the process. The process analysis is based on several assumptions, and the following conditions are adopted:

The process operates under steady-state and steady-flow conditions; the effects of kinetic and potential energy changes are neglected.

Ambient pressure and temperature are set to 101.3 kPa and 300 K, respectively.

Impurities in hydrogen are removed before hydrogen enters the liquefaction process.

Pressure drops in coolers and multi-stream heat exchangers are assumed to be zero.

The physical properties of the working fluids remain constant within the given temperature range.

Kinetic and potential energy terms are excluded from exergy calculations.

The adiabatic efficiency of all compressors is set to 80%, and the mechanical efficiency is set to 0.98.

AMR-based cooling process for hydrogen liquefaction (Case I). Numerical simulations are performed to determine the steady-state refrigeration performance of the three-stage cascaded AMR in the temperature range of 80.5 K to 20 K. Based on this cooling output, a small-scale process is designed to continuously cool atmospheric-pressure hydrogen from 80.5 K to liquefaction. Figures 1 shows the complete HL process. In Aspen Plus V14, heaters and coolers are used to simulate the thermal states of the AMR during magnetization and demagnetization, respectively, with helium as the heat transfer fluid. In Figure 1, each AMR stage is represented by an equivalent hot-end block RH_i and cold-end block RL_i, corresponding to the cycle-averaged heat rejection and cooling capacity obtained from the COMSOL model. Here, i=1, 2, and 3 denote the low-temperature, medium-temperature, and high-temperature stages, respectively. The three cases use the same AMR module and differ only in the precooling strategies.

Under laboratory conditions, using liquid nitrogen as a cold source to precool the hot end of the AMR via a heat exchanger and to cool hydrogen from room temperature to approximately 80 K is a technically simple and easily implementable approach. This system features high practicality, making it particularly suitable for validation experiments of the AMR. However, in practical applications, the nitrogen outlet temperature is far below ambient temperature, resulting in substantial waste of liquid nitrogen cold energy and poor economic performance. Based on the cooling capacity, heat rejection, and pumping work calculated in previous section, the *COP* of this coupled system is 0.215. This value is relatively high for a HL process, but it should be noted that it is achieved at the cost of consuming 51.5 mol/h of liquid nitrogen. To facilitate a fair comparison, the liquid nitrogen consumption is converted into an equivalent power consumption. Using the *SEC* value of 0.84 kWh/L for a small-scale liquid nitrogen production facility from Wang et al.[35] and the density of liquid nitrogen at standard boiling point (806 kg/m^3) obtained from REFPROP, the equivalent power consumption of this liquid nitrogen stream is calculated to be 1503.4 W. After conversion, the equivalent *COP* of the liquid-nitrogen-precooled process is 0.035. Although introducing a small-scale liquid nitrogen generator can ensure continuous refrigeration of the multi-stage AMR, this scheme not only increases system complexity but also results in a low overall *COP* due to insufficient utilization of nitrogen cold energy. Therefore, exploring more economical and efficient heat rejection schemes at the hot end is key to improving the overall system energy efficiency.

MR precooling process (Case II). Although liquid nitrogen precooling offers advantages such as system simplicity and easy accessibility of the cold source, it relies on an external supply of liquid nitrogen, making it difficult to achieve a closed cycle. Moreover, under large-scale operation, it suffers from high consumption and high operating costs, and it is not advantageous from the perspective of system energy efficiency. Therefore, this method is mostly used in experimental studies and is generally not the preferred choice for engineering HL systems. In contrast, the MR cycle, owing to its favorable temperature glide characteristics, is considered an efficient precooling method.[36-37] Based on the study by Ansarinasab et al.[9] and considering the target temperature range, this paper selects a quaternary MR system composed of C1, C2, n-C4, and N_2 to achieve effective thermal matching with the hot end of the AMR and to reduce exergy loss. The MR composition and the corresponding operating parameters are adopted from the literature as a validated baseline and are kept unchanged throughout the comparison. However, this scheme has a drawback: when the above MR is used, the minimum temperature after throttling is only 85 K, which cannot meet the 80.5 K cooling requirement at the hot end of the AMR. To address the issue that the non-azeotropic MR cannot effectively cool the hot end of the high-temperature stage AMR due to the increased phase-change temperature of the light components, this paper removes the C1 component, allowing N_2 to exhibit azeotropic-like characteristics. In this improved MR cycle, N_2 utilizes its azeotropic-like behavior in the low-temperature range to cool the AMR hot end through latent heat exchange at a relatively low phase-change temperature, as shown in Figures 1B.

MR - nitrogen dual-cycle cooperative precooling process (Case III). Since the hot end of the high-temperature stage AMR needs to be stabilized at 80.5 K, the minimum temperature of the MR must be lower than this value. When the aforementioned non-azeotropic MR is used, achieving the required low temperature necessitates a high proportion of light components, which significantly increases the circulating flow rate of the MR cycle and consequently raises the compressor power consumption. Furthermore, due to the removal of a light component, a large temperature difference arises between the heat transfer fluids in the cold-end heat exchangers IIHE3 and HE1 of the precooling cycle, leading to considerable exergy loss. To reduce this temperature difference at the cold end, an independent nitrogen cycle can be added, dedicated to handling the heat rejection load at the hot end of the high-temperature stage AMR, as shown in Figure 1C Since nitrogen after throttling can exist mostly in liquid form, the latent heat exchange can significantly

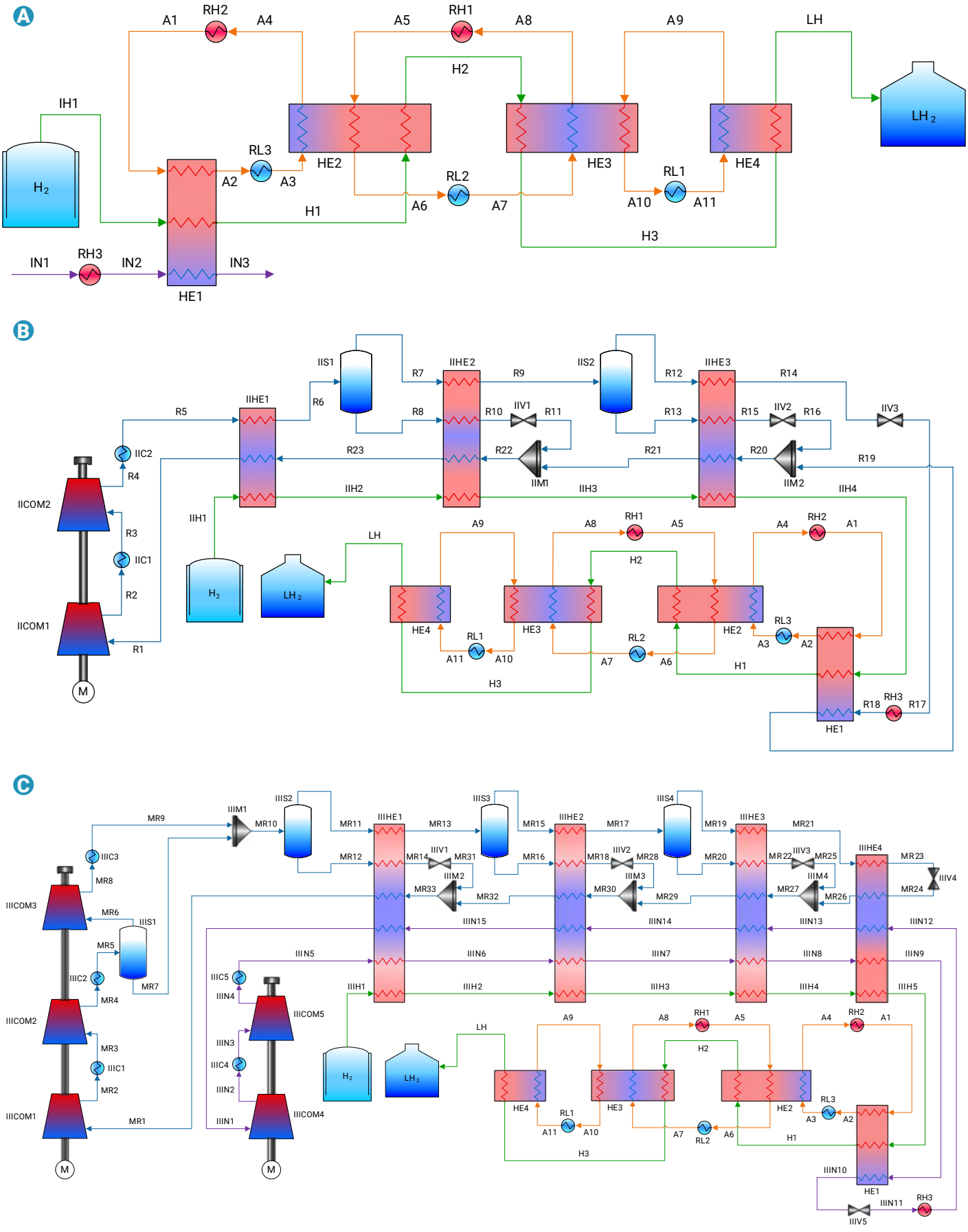


Figure 1. (A)Equivalent model of the AMR low-temperature cooling process. (B) Equivalent model of the MR precooling process. (C) Equivalent model of the MR-nitrogen dual-cycle cooperative precooling process.

reduce the nitrogen flow rate, thereby effectively reducing the compression work of the compressor.

Therefore, the independent nitrogen cycle is not introduced as an additional conventional precooling stage. Its specific function is to remove the concentrated heat-rejection load of the high-temperature AMR at a nearly constant temperature. Meanwhile, the MR composition can be selected primarily according to the broad-temperature hydrogen precooling requirement, without forcing the MR to independently reach the AMR hot-end temperature. This load separation is expected to reduce the MR circulation rate, compression work, and cold-end heat-transfer mismatch.

RESULTS AND DISCUSSION

Performance analysis

Table 2 summarizes the results of energy analysis and exergy analysis for the three processes described above.

The *SEC* and exergy efficiency of the above three processes are shown in Table 2. All processes are designed with the target of producing 1.2 kg/d of liquid hydrogen. The energy consumption of the three-stage AMR is the same for all processes, with values of 0.9 W, 50.0 W, and 236.6 W, and corresponding *COP* values of 0.68, 1.46, and 2.72, respectively.

Under the upstream-inclusive energy boundary, Case III exhibits the best overall energy performance among the three configurations. Its total power consumption is 856.2 W, with an *SEC* of 62 kJ/g and a *COP* of 0.072. These values are better than those of Cases I and II, indicating that the separation of the broad-temperature hydrogen precooling load from the AMR hot-end heat-rejection load effectively reduces the energy required for HL. For Case I, the power required for small-scale liquid-nitrogen production is included in the equivalent power input, resulting in a total power consumption of 1790.9 W and a *COP* of 0.035. However, because upstream liquid-nitrogen production is represented only by an equivalent power consumption rather than by a complete exergy model, the overall exergy efficiency of Case I is not reported. When liquid nitrogen is already available as an external utility, Case I remains attractive for laboratory-scale applications; however, its process-boundary performance is not directly comparable with the closed-cycle configurations. Although Case II eliminates the consumption of an external cryogen, its single MR cycle must simultaneously provide broad-temperature hydrogen precooling and refrigeration near 80.5 K, leading to a high compressor power and an *SEC* of 124 kJ/g. Therefore, Case III provides the most favorable energy performance for the small-scale, continuously operated AMR-based HL system considered in this study.

Sensitivity analysis

Similarly, before optimizing the process parameters of the system, a sensitivity analysis of the key process variables is first conducted to clarify the influence of each parameter on the system energy efficiency. The key operating parameters selected in this study are the intermediate pressure of the two-stage compressor, the inlet pressure of the feed hydrogen, and the adiabatic efficiencies of the compressor and expander.

Through the sensitivity analysis of the two-stage compression intermediate pressure, the system performance of the MR cycle at different intermediate pressures can be obtained, as shown in Figure 2A. The results indicate that as the intermediate pressure increases, both the total compressor power P_t and the *SEC* first decrease and then increase, while the *COP* exhibits the opposite trend. Notably, the *SEC* of the system is less sensitive to the intermediate pressure: when the intermediate pressure increases from 200 kPa to 1250 kPa, the increase in *SEC* relative to its minimum value does not exceed 4%. Even with a single-stage compression scheme, the *SEC* increase is only 4.04%. This indicates that if system miniaturization and structural compactness are the primary goals, adopting single-stage compression does not significantly degrade the *SEC* performance of the system.

The system performance of the nitrogen cycle at different intermediate pressures is shown in Figure 2B. The results indicate that the performance variation trend is the same as that of the MR cycle, and the *SEC* is also less sensitive to the intermediate pressure: the fluctuation of *SEC* is within 3% over the entire operating range. Even when the two-stage compression is simplified to single-stage compression, the *SEC* increase of the system is only 4.11%. This suggests that the marginal benefit of reducing power consumption through two-stage compression is limited for the nitrogen circuit. From a system integration perspective, adopting two-stage compression not only fails to significantly improve energy efficiency but also increases mechanical complexity and initial investment cost. Therefore, using single-stage compression for the nitrogen circuit in this process is more economical and reliable.

Table 2. Summary of energy and exergy analysis results for each precooling process

	Case I	Case II	Case III
W_c (W)	0	1433.4	568.7
W_p (W)	287.5	287.5	287.5
n_{LN2} (mol/h)	51.5	0	0
W_{LN2} (W)	1503.4	0	0
W_{total} (W)	1790.9	1720.9	856.2
LH_2 (g/h)	50	50	50
SEC (kJ/g)	129	124	62
COP	0.035	0.036	0.072
η_{II} (%)	/	11.9	23.9

Figure 3A shows the influence of the feed hydrogen pressure p_{GH1} on the performance indicators of the magnetic refrigeration HL system. The results indicate that regardless of the precooling process employed, the cooling capacity supply in the deep-cooling section of the system matches well with the liquefaction heat load of the feed hydrogen at different pressures, while the system power consumption is mainly controlled by parameters of the magnetic refrigeration cycle itself, such as frequency and magnetic field intensity, and is insensitive to fluctuations in feed hydrogen pressure. This result verifies that the process has excellent thermodynamic robustness under a wide range of feed gas pressure conditions and can maintain a constant energy efficiency level under different inlet conditions.

This study evaluates the system performance at different compressor efficiencies, as shown in Figure 3B. The adiabatic efficiency η of the compressor is selected based on literature data.[38] From Figure 3B, it can be seen that as the adiabatic efficiency increases, both *SEC* and compressor power continuously decrease, while *COP* continuously increases. Specifically, when the efficiency η increases from 0.70 to 0.90, *SEC* decreases from approximately 67.5 kJ/g to 56.9 kJ/g, a reduction of 15.6%; meanwhile, *COP* increases from 0.066 to 0.078, an increase of about 18.5%. This indicates that improving the adiabatic efficiency of the compressor is a key approach to optimizing the energy efficiency of the magnetic refrigeration HL system. By improving compressor performance, not only can the energy consumption required for system operation be significantly reduced, but the overall thermodynamic conversion efficiency can also be markedly enhanced.

Composite curves analysis

In the HL precooling system, the degree of thermal matching within the heat exchanger network has a decisive impact on the overall system energy efficiency. Composite curve analysis is a classical thermodynamic graphical method for evaluating heat transfer performance and identifying sources of irreversibility. This method characterizes the relationship between the temperatures of hot and cold streams and the heat load on a temperature–heat load (T–H) diagram, and can generally be divided into two types: temperature–heat flow composite curves (THCC) and temperature difference composite curves (TDCC).[38]

Figure 4 presents the THCC of the heat exchangers in the precooling process. Overall, the hot- and cold-stream trajectories remain relatively close, indicating favorable heat-capacity-flow-rate matching and effective recovery of internal cooling capacity. However, in the high-heat-load region of approximately 700–850 W, corresponding to IIIHE1, the two curves separate markedly. In this region, the cold composite curve becomes relatively flat, whereas the hot-stream temperature continues to rise almost linearly, indi-

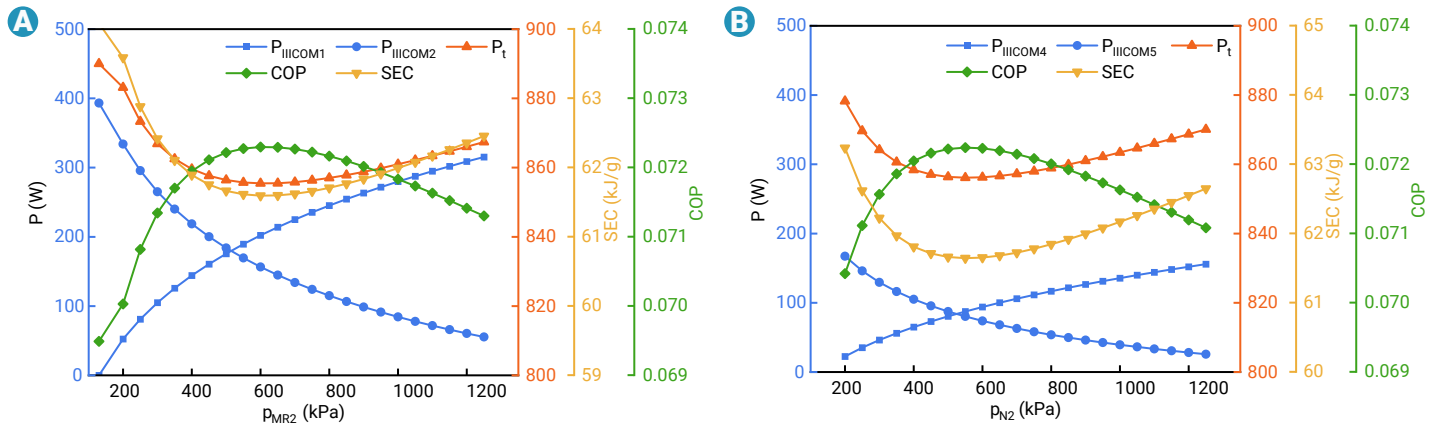


Figure 2. Variation of system performance with process parameters in Case III HL process. (A) Variation of system performance with intermediate pressure in the MR cycle. (B) Variation of system performance with intermediate pressure in the N_2 cycle.

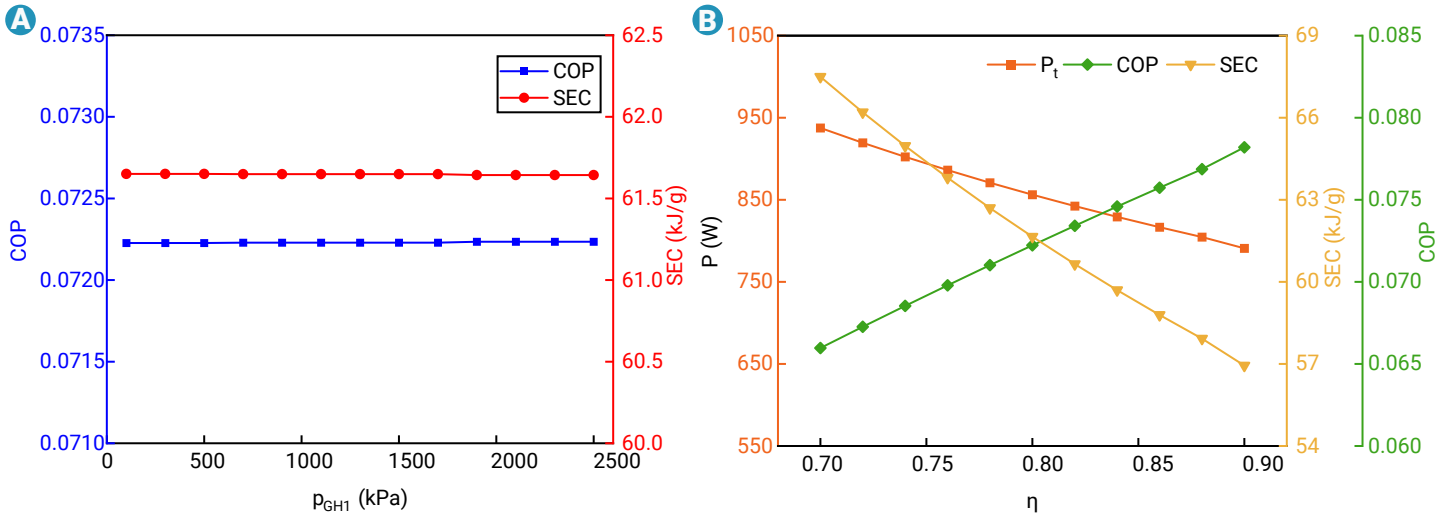


Figure 3. System performance variation with feed hydrogen pressure and compressor adiabatic efficiency. (A) Variation of *COP* and *SEC* with feed hydrogen inlet pressure. (B) Variation of *COP* and *SEC* with adiabatic efficiency.

cating a mismatch between the effective heat-capacity flow rates of hydrogen and the mixed refrigerant. This behavior is mainly associated with the temperature glide of the mixed refrigerant during phase change, which does not fully match the sensible-cooling profile of hydrogen, thereby producing a maximum local temperature difference of approximately 30 K. It should be noted that IIIHE1 is located in the high-temperature section of the MR precooling cycle and is not responsible for heat rejection from the AMR hot end. The independent nitrogen cycle provides near-isothermal heat rejection at approximately 80.5 K and therefore retains its thermal-matching advantage. Among the MR heat exchangers, IIIHE3 exhibits a minimum temperature difference close to 1 K, indicating favorable thermal matching, whereas IIIHE2 and IIIHE4 show intermediate levels of heat-transfer irreversibility. Thus, the dual-cycle configuration achieves good overall thermal integration, while the remaining local irreversibility is mainly concentrated in IIIHE1. Although it could be reduced by adjusting the MR composition or redistributing the cooling load within the MR precooling section, both measures would introduce additional design variables and increase system complexity.

Exergy analysis

Figure 5 presents the exergy destruction distribution of the major components in Case III. The total exergy destruction is 697.55 W, of which the AMR contributes 361.46 W (51.8%), representing the dominant source of irreversibility. This contribution is associated with deep-cryogenic refrigeration near 20 K and the internal irreversibilities arising from finite-temperature regenerative heat transfer, fluid-flow resistance, and the coupling of hydrogen cooling, liquefaction, and ortho-to-para conversion loads. Because the ideal coefficient of performance decreases substantially at such a low refrigeration temperature, the AMR requires a relatively large work input and therefore constitutes the primary target for further system optimization. The heat exchangers and coolers contribute 86.72 W (12.4%) and 78.36 W (11.2%), respectively. The heat-exchanger contribution is consistent with the thermal-matching characteristics identified in Section 4.3, particularly the relatively large temperature differences in IIIHE1 and IIIHE4. The exergy destruction of the MR compressor and the nitrogen compressor is 72.31 W (10.4%) and 25.13 W (3.6%), respectively, accounting for a combined contribution of 14.0%. These losses mainly result from non-isentropic compression and the refrigerant circulation required to provide the precooling load. The gas–liquid separators and throttling valves contribute 57.80 and 15.77 W, respectively, and are therefore secondary optimization targets.

Overall, the exergy analysis identifies the AMR as the principal source of system irreversibility, followed by the heat-exchange network and coolers. Further improvements should therefore prioritize enhancing the intrinsic performance of the AMR through advanced magnetocaloric materials, optimized regenerator geometry, and reduced flow resistance. In parallel, improving the thermal matching in IIIHE1 and IIIHE4 can further reduce heat-transfer irreversibility. Optimization of the remaining components is expected to have a comparatively limited influence on the overall system performance.

CONCLUSION

This paper proposed a HL process integrating an AMR. Three precooling

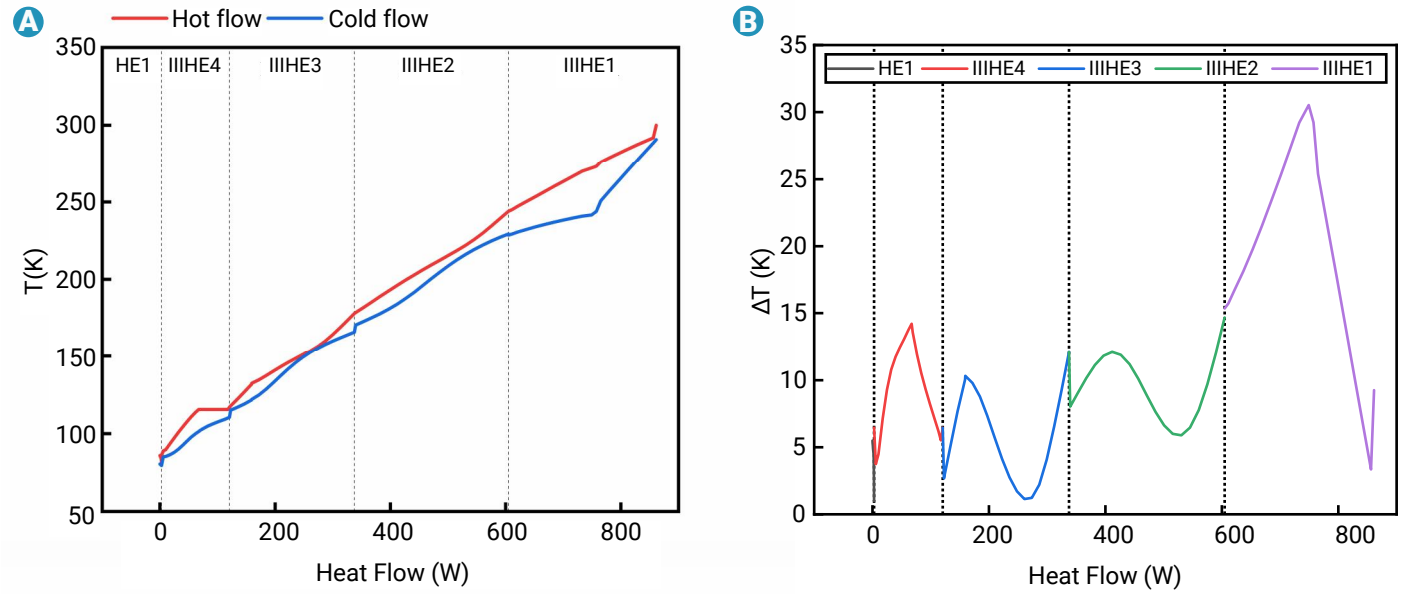


Figure 4. Temperature difference variation curves of heat exchangers. (A) Temperature. (B) Temperature difference.

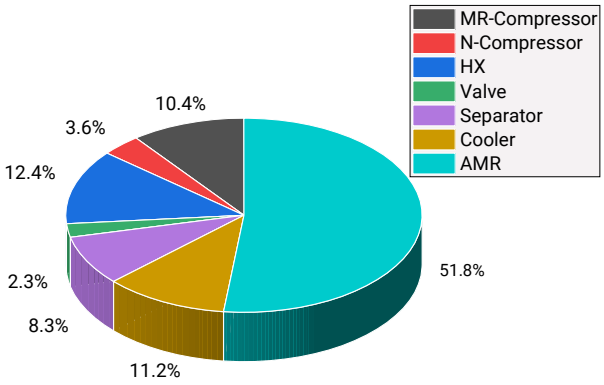


Figure 5. Exergy destruction of major equipment in the AMR-based HL process.

architectures were compared: open-cycle liquid nitrogen (Case I), closed-cycle single MR (Case II), and dual-cycle MR-nitrogen cooperative precooling (Case III). Based on COMSOL simulations of the three-stage cascaded AMR and Aspen Plus process modeling, together with energy and exergy analyses, the following main conclusions are drawn:

(1) Among the three AMR-integrated configurations, Case III achieves the lowest SEC of 62 kJ/g and the highest COP of 0.072. Separating the broad-temperature hydrogen precooling load from the AMR hot-end heat-rejection load reduces the precooling compressor power and improves the overall energy performance.

(2) The system performance is insensitive to hydrogen feed pressure and intermediate compression pressure. Replacing two-stage compression with single-stage compression causes an SEC increase of only approximately 4%, providing an option for system simplification. Compressor adiabatic efficiency remains an important performance parameter.

(3) The exergy analysis shows that the AMR accounts for 51.8% of the total exergy destruction, whereas the heat exchangers, coolers, and compressors contribute 12.4%, 11.2%, and 14.0%, respectively. These results clarify the distribution of irreversibility within the proposed process and confirm that the dominant losses are concentrated in the deep-cryogenic AMR and local heat-transfer mismatch rather than in the precooling compressors.

In summary, Case III demonstrates high energy efficiency, compactness, and operational flexibility. These findings support the development of distributed, modular magnetic refrigeration HL systems. The conclusions of this study are limited to the small-scale AMR-integrated system and the operating assumptions. The results should not be interpreted as a direct performance ranking between AMR-based systems and conventional industrial-scale Claude HL processes.

REFERENCES

1. Pells R. (2025). How a hydrogen lab is helping to power Spain's green-energy shift. *Nature*. DOI:10.1038/d41586-025-01025-y
2. Zhang T., Uratani J., Huang Y., et al. (2023). Hydrogen liquefaction and storage: Recent progress and perspectives. *Renew. Sustain. Energy Rev.* **176**:113204. DOI:10.1016/j.rser.2023.113204
3. Li J., Liu J., Dai H., et al. (2024). Rapid development of hydrogen in the energy sector raises safety regulatory concerns. *Innov. Energy* **1**:100037. DOI:10.59717/j.xinn-energy.2024.100037
4. International Energy Agency. (2021). Net Zero by 2050. *IEA*.
5. Petitpas G. (2018). Simulation of boil-off losses during transfer at a LH2 based hydrogen refueling station. *Int. J. Hydrog. Energy* **43**:21451–21463. DOI:10.1016/j.ijhydene.2018.09.132
6. Fang L., Dong X., Wang H., et al. (2025). Economic analysis of compressed gaseous hydrogen, liquid hydrogen, and cryo-compressed hydrogen storage methods for large-scale storage and transportation. *Int. J. Hydrog. Energy* **162**:150725. DOI:10.1016/j.ijhydene.2025.150725
7. Zhou B. (2024). Liquid hydrogen carriers: Linking renewable energies for a carbon-neutral future. *Innov. Energy* **1**:100020. DOI:10.59717/j.xinn-energy.2024.100020
8. Ahmad A., Nnabuife S.G., Oko E., et al. (2025). Comprehensive review of advances and challenges in hydrogen liquefaction. *Sustain.* **6**:100192. DOI:10.1016/j.nxsust.2025.100192
9. Ansarinasab H., Fatimah M. and Khojasteh-Salkuyeh Y. (2023). Conceptual design of two novel hydrogen liquefaction processes using a multistage active magnetic refrigeration system. *Appl. Therm. Eng.* **230**:120771. DOI:10.1016/j.applthermaleng.2023.120771
10. Aasadnia M. and Mehrpooya M. (2018). Large-scale liquid hydrogen production methods and approaches: A review. *Appl. Energy* **212**:57–83. DOI:10.1016/j.apenergy.2017.12.033
11. Taghavi M., Colpan C.O. and Dincer I. (2026). Development of an integrated production and liquefaction system of hydrogen and green natural gas: energy, exergy, economic and sensitivity assessments. *Energy* **360**:141476. DOI:10.1016/j.energy.2026.141476
12. Taghavi M. and Lee C.-J. (2025). Development of a novel hydrogen liquefaction structure based on liquefied natural gas regasification operations and solid oxide fuel cell: Exergy and economic analyses. *Fuel* **384**:133826. DOI:10.1016/j.fuel.2024.133826
13. Zhang R., Cao X., Ai D., et al. (2025). Analysis of a novel hydrogen liquefaction process based on a mixed refrigerant Brayton cryogenic cycle utilizing LNG cooling: energy, exergy, economy and environment. *Energy* **336**:138424. DOI:10.1016/j.energy.2025.138424
14. International Energy Agency. (2023). Global Hydrogen Review 2023. *IEA*.
15. Eom S., Kim S., Han G., et al. (2026). Low-cost green hydrogen from renewable energy curtailment: A techno-economic analysis with a real-time AI-driven approach. *Energy* **349**:140569. DOI:10.1016/j.energy.2026.140569
16. International Renewable Energy Agency. (2022). Innovation outlook: Renewable

ammonia. *IRENA*.
17. Park J., Ryu K.H., Kim C.-H., et al. (2023). Green hydrogen to tackle the power curtailment: Meteorological data-based capacity factor and techno-economic analysis. *Appl. Energy* **340**:121016. DOI:10.1016/j.apenergy.2023.121016
18. Handayani W., Zhu X. and Cooke F.L. (2025). Mapping hydrogen demand for heavy-duty vehicles: a spatial disaggregation approach. *Energy Inform.* **8**:91. DOI:10.1186/s42162-025-00550-4
19. Semchukova V., Topolski K. and Abdin Z. (2025). Hydrogen technology for maritime applications: A review of challenges, opportunities, and lessons from the port authority of New York and New Jersey. *Renew. Sustain. Energy Rev.* **216**:115641. DOI:10.1016/j.rser.2025.115641
20. Liu Y., Su X., Fang L., et al. (2025). Large cryogenic magnetocaloric effect of the Laves-phase Ho(1-x)Dy(x)Al(2) compounds within liquid hydrogen temperature range. *J. Alloys Compd.* **1010**:178324. DOI:10.1016/j.jallcom.2024.178324
21. Yu B.F., Gao Q., Zhang B., et al. (2003). Review on research of room temperature magnetic refrigeration. *Int. J. Refrig.* **26**:622–636. DOI:10.1016/S0140-7007(03)00048-3
22. Kamiya K., Natsume K., Uchida A., et al. (2025). Hydrogen liquefaction by active magnetic regenerative refrigeration. *Cryogenics* **152**:104205. DOI:10.1016/j.cryogenics.2025.104205
23. Belkadi M. and Smaili A. (2021). Comparative Study between precooled Claude Liquefaction Cycle and an Active Magnetic Regeneration Cycle applied to Hydrogen Liquefaction. *ENP Eng. Sci. J.* **1**:9–16. DOI:10.53907/enpesj.v1i2.12
24. Esmaeilzadeh A., Javaherdeh K., Naghashzadegan M., et al. (2026). Conceptual design and analysis of a boil-off gas re-liquefaction process driven by a multi-stage active magnetic regenerative cryocooler. *Appl. Therm. Eng.* **289**:129987. DOI:10.1016/j.applthermaleng.2026.129987
25. Ansarinasab H., Fatimah M. and Khojasteh-Salkuyeh Y. (2023). Performance improvement of air liquefaction processes for liquid air energy storage (LAES) using magnetic refrigeration system. *J. Energy Storage* **65**:107304. DOI:10.1016/j.est.2023.107304
26. Liponi A., Tenda M., Bjørk R., et al. (2025). Analysis of configurations for coupling an active magnetic regenerator with heat exchangers for hydrogen liquefaction. *Fuel Process. Technol.* **278**:108337. DOI:10.1016/j.fuproc.2025.108337
27. Zheng W., Shen J., Li Z., et al. (2024). Numerical simulation of a multistage magnetic refrigeration system in the temperature range of liquid hydrogen. *Int. J. Hydrog. Energy* **51**:523–535. DOI:10.1016/j.ijhydene.2023.07.192
28. Kamiya K., Matsumoto K., Numazawa T., et al. (2022). Active magnetic regenerative refrigeration using superconducting solenoid for hydrogen liquefaction. *Appl. Phys. Express* **15**:053001. DOI:10.35848/1882-0786/ac5723
29. Sun S., Jiang W., Yang F., et al. (2026). Optimization and analysis of a new liquefied natural gas and nitrogen cascade pre-cooling hydrogen liquefaction process. *Cryogenics* **153**:104253. DOI:10.1016/j.cryogenics.2025.104253
30. Ribeiro P.O., Alho B.P., Oliveira R.S.D., et al. (2022). Magnetothermal properties of Ho(1-x)Dy(x)Al(2) (x = 0, 0.05, 0.10, 0.15, 0.25 and 0.50) compounds. *J. Magn. Magn. Mater.* **544**:168705. DOI:10.1016/j.jmmm.2021.168705
31. Bykov E., Liu W., Skokov K., et al. (2021). Magnetocaloric effect in the Laves-phase Ho(1-x)Dy(x)Al(2) family in high magnetic fields. *Phys. Rev. Mater.* **5**:095405. DOI:10.1103/PhysRevMaterials.5.095405
32. Nielsen K.K., Bahl C.R.H., Smith A., et al. (2010). A comprehensive parameter study of an active magnetic regenerator using a 2D numerical model. *Int. J. Refrig.* **33**:753–764. DOI:10.1016/j.ijrefrig.2009.12.024
33. Xu Y., Bi Y. and Ju Y. (2024). The thermodynamic analysis on the catalytical ortho-para hydrogen conversion during the hydrogen liquefaction process. *Int. J. Hydrog. Energy* **54**:1329–1342. DOI:10.1016/j.ijhydene.2023.11.259
34. Aghabalazadeh M., Garousi Farshi L. and Mosaffa A.H. (2026). Design and performance analysis of an improved Claude-cycle-based hydrogen liquefaction system. *Energy Convers. Manag.* **352**:121060. DOI:10.1016/j.enconman.2026.121060
35. Wang H.C., Guo H., Chen G.F., et al. (2018). Thermodynamic design and analysis of movable small scale mixed-refrigerant liquid nitrogen generators. *Int. J. Refrig.* **90**:202–215. DOI:10.1016/j.ijrefrig.2018.04.010
36. Sleiti A.K., Al-Ammari W.A. and Ghani S. (2023). Novel dual-mixed refrigerant precooling process for high capacity hydrogen liquefaction plants with superior performance. *J. Energy Storage* **66**:107471. DOI:10.1016/j.est.2023.107471
37. Petri G., Andreini N., Milazzo A., et al. (2026). Thermodynamic analysis of a dual mixed-refrigerant hydrogen liquefaction process with continuous ortho–para conversion method. *Int. J. Hydrog. Energy* **205**:153386. DOI:10.1016/j.ijhydene.2026.153386
38. Liu C. and Zhang J. (2025). Introducing and energy analysis of a new hydrogen liquefaction process using different percentage of LNG as a cold source supplement. *Int. J. Hydrog. Energy* **167**:150975. DOI:10.1016/j.ijhydene.2025.150975

FUNDING AND ACKNOWLEDGMENTS

This work is supported by the Natural Science Foundation of China (No. U22B20112).

AUTHOR CONTRIBUTIONS

Zhouhang Hu: Conceptualization, Writing – Original Draft, Formal Analysis, Modeling, Data Curation, Validation. Zhenxing Li: Data Curation, Methodology, Software, Resources, Writing – Review & Editing. Yakun Liu: Methodology, Software. Jun Liu: Investigation, Data Curation, Validation. Huifang Kang: Investigation, Visualization. Hang Li: Investigation, Data Curation. Hongwei Zhang: Investigation. Jiahui Wang: Formal Analysis. Jun Shen: Supervision, Project Administration, Resources, Funding Acquisition.

DECLARATION OF INTERESTS

Jun Shen (full name) is an Editorial Board member of The Innovation Energy and was blinded from reviewing or making final decisions on the manuscript. Peer review was handled independently of this member and their research group. The other authors declare no conflicts of interest.

DATA AND CODE AVAILABILITY

Data are available from the corresponding author upon reasonable request.

SUPPLEMENTAL INFORMATION

It can be found online at https://doi.org/10.59717/j.xinn-energy.2026.100187